J1.9 THE TURBULENT STRUCTURE OF THE POLAR STABLE BOUNDARY LAYER: WAVELET TRANSFORMATION AND MULTIRESOLUTION FLUX DECOMPOSITION

Aline van den Kroonenberg and Jens Bange

Institute of Aerospace Systems at Technical University Braunschweig, Germany

1. INTRODUCTION

In general a turbulent flow can be divided into scale regimes. The large scales, contain most of the energy and are responsible for the transport of heat, momentum and mass. The small scales include the dissipation range and the inertial range (Sreenivasan and Antonia 1997). Knowledge of small scale turbulence is mostly based on Kolmogorov's theory (Kolmogorov 1941), but no global theory of turbulence is present. Within the stable boundary layer the turbulent fluxes are small and therefore easily affected by mesoscale fluxes. To estimate this mesoscale flux correctly, long averaging times are needed. Small scale turbulence has completely different characteristics compared to the mesoscales. As small scale turbulence is related to wind shear and temperature stratification, the mesoscales are not. For the proper investigation of small scale turbulence, especially in the (very) stable boundary layer, any contamination of mesoscale fluxes in the records should be expelled (Mahrt and Vickers 2006).

In the polar stable boundary layer (PSBL) weak turbulence was observed. Any contribution of mesoscale fluxes may result in large relative errors or even in a change of sign of the calculated turbulent fluxes. Within this PSBL study the flight durations were not long enough to resolve these mesoscale fluxes properly. Therefore, any contribution of these mesoscale fluxes were expelled from the turbulent flux measurements. The proper averaging time scale was investigated by using multiresolution (MR) flux decomposition (Howell and Mahrt 1997; Vickers and Mahrt 2003; Vickers and Mahrt 2006). A gap scale was defined which divided the turbulent and the mesoscale flux within the flow.

A second method to decompose a turbulent time series is the wavelet transformation. The time series is decomposed into a time-frequency space, which gives the opportunity to determine both the dominant modes of variability and how these modes vary in time (Torrence and Compo 1998; Feigenwinter 1999). The wavelet transformation is able to detect isolated events and preserve information about their occurrence and characteristics. The wavelet method was compared to the Fourier method in a couple of studies (e.g., Katul and Parlange 1994; Strunin and Hiyama 2004). The main advantage of the wavelet method is not only a localisation for frequencies (as for Fourier transformations) but also for time and space. The localisation in space is particularly important for studies of non-homogeneous turbulence. The wavelet method was also successfully used to detect coherent structures in the convective boundary layer (e.g., Hagelberg and Gamage 1994; Collineau *et al.* 1993) and waves in the stable boundary layer (SBL) (Rees *et al.* 2001).

Both methods were used to define the gap time scales of the turbulent fluxes measured in the PSBL. Measurements were made by the helicopter-borne turbulence probe Helipod. The flights were performed at low altitudes above the surface (10-60 m) which was particularly useful in the shallow SBL.

The database used for this study was obtained during an Arctic campaign (ARK-XII Jul-Sep 1996) which was carried out with the German research vessel Polarstern. Within this campaign, Helipod flights were performed over the Kara Sea, Laptew Sea and East-Siberian Sea. In total 5 flights over sea ice were analysed for this study. A low level jet (LLJ) was present during all the measurements at a height of about 100 m. During one day a strong LLJ (22 m s^{-1}) occurred at 250 m.

Within this study the portion of the mesoscale fluxes to the total sensible heat and moisture flux was investigated. During most of the flights the wind was weak. Small heat and moisture fluxes were measured. Multiresolution decomposition was used to define a gap scale for these turbulent fluxes. These gap scales were used as the averaging time scale to calculate the fluxes. Cross wavelet spectra and cross wavelet power

Corresponding author: Aline van den Kroonenberg, Aerospace Systems, Technical University of Braunschweig, Germany; e-mail: a.kroonenberg@tu-bs.de

spectra were used to verify the time scales found by MR cospectra.

2. MEASUREMENT SYSTEM AND OBSERVATIONS

The Helipod is a helicopter-borne, high resolution meteorological measurement system (Muschinski and Wode 1998; Bange and Roth 1999; Bange *et al.* 2002). The system was designed for in-situ measurements of small scale turbulent fluctuations of wind, temperature, humidity and the associated turbulent fluxes. The Helipod is 5 m in length, carried by a helicopter on a 15 m rope at an airspeed of 40 m s^{-1}.

Fig. 1: Helicopter borne turbulence probe Helipod during take off from the research vessel Polarstern.

To achieve a high temporal resolution, every meteorological variable was measured with at least two different types of instruments. One sensor, with a short response time and the disadvantage of a temporal drift, sampled at 100 Hz. The other sensor, with a slow response but with a high accuracy on a large time scale, sampled at 20 Hz. The two datasets were combined by complementary filters which resulted in accurate 100 Hz time series of the meteorological parameters. The Helipod was equipped with a five hole probe, an inertial navigation system (INS) and two GPS antennas and receivers. The navigation systems were complemented by a radar altimeter. The temperature was measured with a Rosemount resistance thermometer and a fast open wire element. The humidity was measured by a Lyman Alpha hygrometer, a capacitive sensor (Humicap) and a dew point mirror. This sensor package was used to determine the static pressure, the true air speed, the position, the attitude and finally the wind vector.

The ARK-XII expedition with the research vessel Polarstern was carried out in July to September, 1996, in Kara, Laptew and East Siberian Sea. Several flight strategies were flown containing horizontal legs and vertical profiles. The vertical profiles provided information about the evolution of temperature, humidity, wind speed and wind direction with height (stratification, presence of LLJ). From the horizontal flight legs the turbulent fluxes and (co-)variances were calculated. The 'box' flight pattern consisted of four legs flown in a square shaped pattern. These boxes were flown at several altitudes. The 'U-shaped' pattern contained several legs flown in an U-shape at one altitude.

3. MULTIRESOLUTION FLUX DECOMPOSITION

Multiresolution (MR) analysis applied to time series decomposes the data into averages on different time scales and represents a simple orthogonal decomposition. The MR spectra yield information on the scale dependence of the variance as for Fourier spectra. Unlike Fourier spectra, the MR spectra satisfy Reynold's averaging at all scales and do not assume periodicity (Howell and Mahrt 1997; Vickers and Mahrt 2003). The location of the peak in MR spectra in time scale domain depends primary on the time scale of the fluctuations, while the peak of the Fourier spectra depends on the periodicity.

MR decomposition divides the data record into simple averages on different scales (segments) of width $1,2,4,...2^M$ consecutive data points. The lowest order mode is the simple average over the record, which is then removed. The next mode consists of the means of the two half records, which are then removed, and so forth. This can be interpreted as a high pass filter which at each application removes increasingly shorter averaging time scale fluctuations.

For a scale m the averaging segment of width 2^m points are sequenced as $n = 1,2,...2^{M-m}$, where n identifies the position of the segment within the series. The average for the n'th segment at scale m is given by

$$\overline{\omega}_n(m) = \frac{1}{2^m} \sum_{i=I}^{J} \omega r_i(m) \quad , \tag{1}$$

in which $I = (n-1)2^m + 1$ and $J = n2^m$.

The MR cospectra for time series ϕ and γ,

$$\mathrm{MR}_{\phi\gamma}(m+1) = \frac{1}{2^{M-m}} \sum_{n=1}^{2^{M-m}} \overline{\phi}_n(m)\, \overline{\gamma}_n(m) \quad . \quad (2)$$

3.1 Modification of the data grid

To perform a MR decomposition, a record length of $R = 2^M$ data points is required. There are two ways to accomplish this:

1. Discard some data points,
2. Interpolate the original time series on a finer grid.

Preferred is the second method (described by Howell and Mahrt 1997), while no data points will be lost. But to make some comparison or build some averages between the records, the first method is recommended. To build an average, all the time series should have the same length. To achieve this, the maximum 2^M was calculated from the shortest leg.

$$2^M \leq R < 2^{M+1} \quad , \quad (3)$$

where R is the number of data points from the shortest time series. The new length of all the legs will be 2^M.

3.2 Defining a gap scale

Vickers and Mahrt (2003) defined a cospectral gap scale, which was used to separate turbulence from mesoscale motions. An algorithm was written which scanned the cospectrum starting at the smallest scale. The gap scale occurred at a longer time scale than the first peak in the cospectrum which was associated with turbulence. One of the following conditions for detection of the gap scale was required:

- The accumulative flux changed by less then 1% with an increase in time scale,
- The cospectrum changed sign (zero crossing).

The accumulative flux was calculated by summing up the contributions to the flux starting at the smallest scale.

4. WAVELET TRANSFORMATION

The continuous wavelet transformation $W_n(s)$ of a real square integrable signal x_n with respect to an analysing wavelet $\psi_0(\eta)$ can be defined by

$$W_n(s) = \sum_{n'=0}^{N-1} x_{n'} \psi^* \left[\frac{(n'-n)\delta t}{s} \right] \quad , \quad (4)$$

where the $(*)$ indicates the complex conjugate and x_n a time series with equal time spacing δt and $n = 0...N-1$. By varying the wavelet scale s and translation along the localised time index n, a diagram can be constructed showing both the amplitude of any feature versus the scale and how this amplitude varies with time. The wavelet function $\psi_0(\eta)$ is normalised to make it comparable at each scale s to each other and to the transformations of other series.

Here the nonorthogonal complex Morlet wavelet (6th order) was chosen. The Morlet wavelet was found to be suitable for statistical analysis and for pattern recognition in turbulence data (Strunin and Hiyama 2004; Salmond 2005). The chosen order m = 6 was optimal and provided good time localisation and frequency resolution. This good resolution in Fourier space was needed to define the gap between turbulence and mesoscale.

4.1 Wavelet power spectrum

The wavelet power spectrum is defined as the wavelet transformation of the autocorrelation function

$$WPS_n(s) = W_n(s)\, W_n^*(s) \Longrightarrow |W_n(s)|^2 \quad , \quad (5)$$

where $W_n^*(s)$ is the complex conjugate of $W_n(s)$.

The wavelet power is normalised with the variance of the time series to make it relative to white noise.

For the wavelet transformation, a set of scales (s) is needed. The scales are written as fractional powers of two

$$s_j = s_0\, 2^{j\delta j} \qquad j = 0, 1, ..., J \quad (6)$$

in which s_0 is the smallest resolvable scale, δj the spacing between the scales (0.25 for logarithmic units) and J the largest scale.

In theory the time series can be completely decomposed using a maximum of levels (k), $N = 2^k$, where N is the series length,

$$J\delta j = \log_2 \left(\frac{N \cdot s_0^{-1}}{\mathrm{FP}} \right) \quad , \quad (7)$$

in which the Fourier period (FP) is different for every wavelet type. But for the most purposes a

partial decomposition is sufficient The FP (in sec) represents the relationship between the Fourier period and the wavelet scale. The FP for the Morlet (6th order) wavelet is almost 1, which indicates that the wavelet scale almost equals the Fourier period,

$$\text{Morlet FP} = \frac{4\pi}{m + \sqrt{2 + m^2}} \quad , \tag{8}$$

in which m is again the wavelet order (Torrence and Compo 1998).

4.2 Cross Wavelet

Two time series X and Y can be compared by cross wavelet analysis. The cross wavelet spectrum is defined as (Torrence and Compo 1998; Maraun and Kurths 2004)

$$WC_n^{XY}(s) = W_n^X(s)\, W_n^{Y*}(s) \quad , \tag{9}$$

and the cross wavelet power spectrum

$$WCP_n^{XY}(s) = \left| W_n^X(s)\, W_n^{Y*}(s) \right| \quad . \tag{10}$$

4.3 Wavelet covariance

The covariance of two variables can be calculated as the multiplication of both wavelet real parts (Attié and Durand 2003)

$$CW_n^{XY}(s) = \Re\left(W_n^X(s)\right)\, \Re\left(W_n^Y(s)\right) \tag{11}$$

If one of the signals is the vertical velocity, the covariance corresponds to the vertical turbulent flux.

5. RESULTS

Of all the measurements made during the ARK XII campaign, five flights were analysed more detailed. On three days (flight no. 03, 06, 18) a 'box' pattern was flown (Tab.1). During flight no. 05 a 'U-shaped' flight pattern was performed at an altitude of approximately 10 m. Two horizontal legs were flown during flight 04. A LLJ was present on all the measurement days. During flight no. 18 this LLJ was stronger compared to the other flights and had its maximum at 250 m height. During the first 4 flights, the boundary layer was stably stratified up to 100 m height. On the last flight day (no. 18) the stable boundary layer reached a height of 250 m.

5.1 MR gap scale defined for the heat flux

To define a gap scale, first the multiresolution cospectrum of the kinematic heat flux $\overline{w'\theta'}$ was calculated. The decompositions were made on time series with the same duration. In this study a length of 2^{14} data points, which represented 163.84 s or $\approx$ 6.5 km, was chosen. Long flight legs were divided into sections of 163.84 s. For shorter legs some data points were discarded to obtain the required length. With these decompositions the averaged cospectra for every 'box' or 'U-shaped' flight pattern were calculated.

The first peak in the MR cospectra was related to the turbulent transport. Figure 2 shows for most of the flights a constant time scale of $\approx$ 0.32 s independent of the magnitudes of the measured fluxes (between -1 and -15 $\mathrm{Wm^{-2}}$). Using the operation speed of the Helipod of 40 m $\mathrm{s^{-1}}$, a corresponding peak scale of 12-13 m was found. For almost all the flights, the value of P did not exceed the value of the height z above the surface.

During flight no. 18 larger time scales of 0.6-1.28 were estimated. On this day a strong LLJ was observed with a wind maximum of 22 m $\mathrm{s^{-1}}$(Tab. 1).

Tab. 1: Analysed flight days. h_{LLJ} represents the height of the low level jet maximum and v_{LLJ} the corresponding velocity.

No.	Date	Levels [m]	h_{LLJ} [m]	v_{LLJ} [m $\mathrm{s^{-1}}$]
03	27.07.96	11, 31	140	5
04	28.07.96	11	80, 100	8
05	28.07.96	11, 12	100	12
06	30.07.96	11, 31, 62	100	10
18	27.08.96	12, 46	250	22

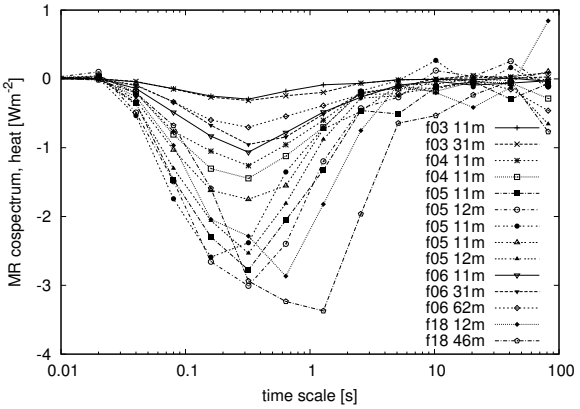

Fig. 2: Averaged MR cospectra, $\mathrm{MR}_{w'\theta'}$. For every flight pattern at a certain height (Tab. 2), the averaged $\mathrm{MR}_{w'\theta'}$ was calculated.

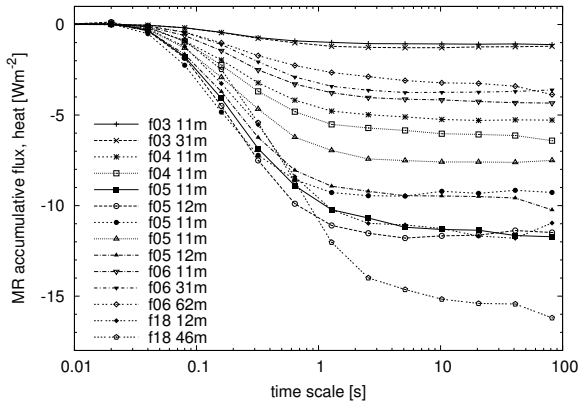

Fig. 3: Accumulated MR flux, $\overline{w'\theta'}$. The flux was calculated by summing up the contributions to the flux (Fig 2) starting at the smallest time scale.

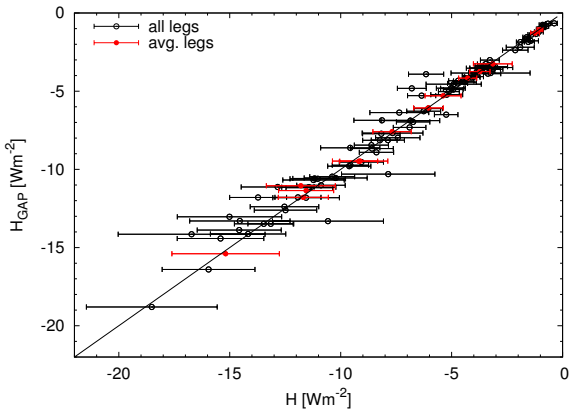

Fig. 4: The heat flux estimated over the whole record H compared to heat flux estimated using the gap time scale H_{gap} in Wm^{-2}. The open dots represent all the legs, the close red dots represent the averages (also described in Tab. 2).

A strong LLJ produces a shear layer between the surface and the wind maximum, which is responsible for the generation of turbulence (Newsom and Banta 2003; Banta *et al.* 2003). Due to the strong wind a significant heat flux H was measured at the flight level of 12 m which increased significantly aloft (see Tab. 2). This type of boundary layer is called an upside-down boundary layer where turbulence is generated at the top due to strong shear of the LLJ (Mahrt 1999).

The cospectral gap time scale was used to separate turbulence from mesoscale motions and included therefore the complete turbulent flux. The gap had a time scale larger than the cospectral peak and was identified when the cospectrum crossed zero or the accumulative flux did not significantly change with increasing time scale. The estimated gap time scales (G_{mr}) are listed in Tab. 2. No obvious dependence of G_{mr} on the magnitude of the heat flux, stratification, the measurement height or even the LLJ height (Tab. 1) was found. The gap time scales were estimated between 5 and 30 s, which corresponded to a length between 200 and 1200 m. If larger averaging time scales were used for the flux calculation, such as the total time series length, the mesoscale fluxes could affect the estimated fluxes.

Tab. 2: Spectral gap scales for the averaged MR cospectra $\overline{w'\theta'}$ over a box or a couple of legs in the same altitude, z. H is the heat flux for the whole record, H_{gap} is the heat flux calculated using the gap time scale (G_{mr}). The main transporting eddies were found at time scale P.

No.	avg.	z	H	H_{gap}	G_{mr}	P
		m	Wm^{-2}	Wm^{-2}	s	s
03	box	11	-1.02	-1.06	5.12	0.3
03	box	31	-1.24	-1.28	8	0.3
04	leg	11	-5.39	-5.30	30	0.32
04	leg	11	-6.05	-6.07	20.5	0.32
05	leg	11	-11.56	-11.36	20.5	0.32
05	leg	12	-11.69	-11.79	8	0.32
05	leg	11	-9.19	-9.48	5.2	0.18
05	leg	11	-7.69	-7.59	20	0.32
05	leg	12	-9.13	-9.47	10.2	0.32
06	box	11	-4.28	-4.16	10	0.32
06	box	31	-3.73	-3.74	10.2	0.35
06	box	62	-3.14	-3.25	20.5	0.32
18	box	12	-11.80	-11.05	6	0.64
18	box	46	-15.19	-15.40	30	1.28

For the averaged cospectra, there were no large differences between H and H_{gap} ($H - H_{\mathrm{gap}} = \Delta H$, see also Fig. 3). Larger values for ΔH were found for the single cospectra, but the absolute $|\Delta H|$ remained smaller then 3 Wm^{-2} (Fig 4). The values for ΔH were mostly negative. This indicated a negative contribution by the mesoscale flux to the heat flux. Only two exceptions in the measurements occurred where H was clearly influenced by the a positive mesoscale flux. As the mesoscale transport was mainly based on advection, the source for the upwards flux could be open water (which was warmer than sea ice) at a certain distance from the measurement site.

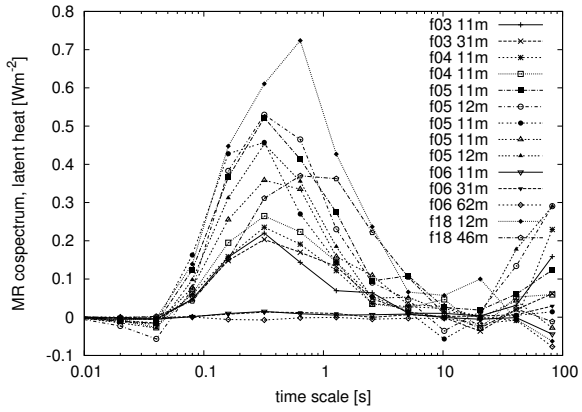

Fig. 5: Averaged MR cospectra, $\mathrm{MR}_{w'm'}$

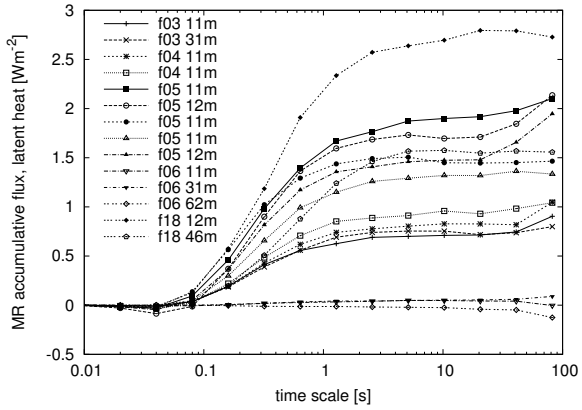

Fig. 6: Accumulated MR flux, $\overline{w'm'}$

5.2 MR gap scale defined for the latent heat flux

The latent heat flux $\overline{w'm'}$ over sea ice was small and directed upwards. Small values of $\overline{w'm'}$ were found in a range between 0.7 and 2.8 Wm^{-2}.

The gap time scales were also defined for the MR decompositions of the kinematic moisture fluxes, $\overline{w'm'}$. For flight no. 06 no gap scales were defined due to the very small magnitudes of the fluxes ($\overline{w'm'} \leq 0.05\ \mathrm{Wm}^{-2}$). The gap scales varied mainly between 10 and 20 s (Tab. 3), which was a more steady value range compared to the gap scales for $\overline{w'\theta'}$ (Tab. 2). While the magnitudes of the latent heat fluxes were small, the influences of the mesoscale fluxes were hard to recognise.

The time scale P was found to be similar compared to the cospectral peak for $\overline{w'\theta'}$ (Fig. 5). This indicated that the main transport of the turbulent eddies had the same time scale for both latent and sensible heat flux. Again for flight no. 18 a slightly larger time scale P was found compared to the other flights. Due to the stronger shear conditions during this day, turbulence was stronger which corresponded to a larger time scale.

Tab. 3: Spectral gap scales for the averaged MR cospectra $\overline{w'm'}$ over a box or a couple of legs in the same altitude, z. E is the latent heat flux for the whole record, E_{gap} is the latent heat flux calculated using the gap time scale (G_{mr}). The main transporting eddies were found at time scale P.

No.	avg.	z	E	E_{gap}	G_{mr}	P
		m	Wm^{-2}	Wm^{-2}	s	s
03	box	11	0.68	0.71	20.5	0.32
03	box	31	0.71	0.75	10.2	0.32
04	leg	11	0.80	0.83	20.5	0.32
04	leg	11	0.94	0.96	14	0.32
05	leg	11	1.96	1.92	20.5	0.32
05	leg	12	1.79	1.71	20.5	0.32
05	leg	11	1.44	1.51	6	0.3
05	leg	11	1.37	1.32	20.5	0.32
05	leg	12	1.43	1.48	20.5	0.32
18	box	12	2.80	2.70	6	0.64
18	box	46	1.51	1.58	11	0.7

Table 3 shows small influences of the mesoscale fluxes (E - E_{gap}). For the averaged flight legs, these differences were not significant (see also Fig. 6). Considering again the single cospectra, small differences between E and E_{gap} were found but not larger then 0.5 Wm^{-2} (Fig. 7).

5.3 Wavelet gap scale

Wavelet analysis was used to decompose the turbulent flow into time and frequency space. The variability in time and space gave information about the homogeneity of the turbulent flow. The gap time scale of intermittent turbulence was highly affected by the turbulent outbursts, therefore only continuous turbulence was analysed. The decomposition in frequency space gave information about the turbulence scales and was compared with the scales estimated by MR decomposition.

In Fig. 9 the cross wavelet and the wavelet covariance of $\overline{w'\theta'}$ are shown for one single leg (day 05, leg 02). The corresponding MR decomposition of $\overline{w'\theta'}$ is shown in Fig. 8. For this particular leg, the MR cospectral gap time scale was detected around 7 s. At this time scale the MR cospectra crossed zero. A positive contribution to the $\overline{w'\theta'}$ flux was present at the averaging time sca-

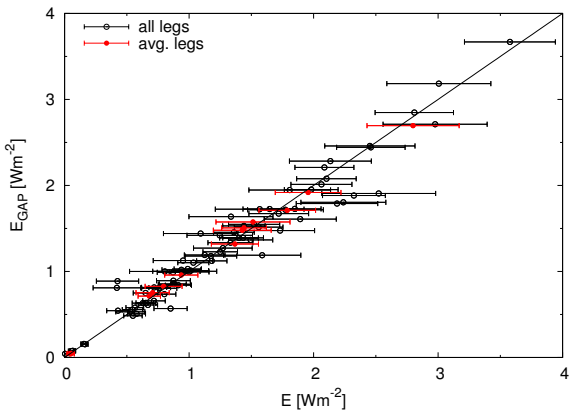

Fig. 7: The latent heat flux E estimated over the whole record compared to the latent heat flux E_{gap} estimated using the gap time scale in Wm^{-2}. The open dots represent all the legs, the close dots represent the averages (also described in Tab. 3).

le of 10 s (Fig. 8). Again a negative contribution predominated at a time scale of 20 s. Both events were visible in the cross wavelet spectra and covariance. A gap time scale was not easily defined using wavelet transformation only. Nevertheless, the MR gap time scale was confirmed by the wavelet covariance. The transition from the negative flux into a positive contribution to the heat flux was clearly visible at a wavelength of 7 s (Fig. 9).

For the moisture flux a gap scale of 8 s was estimated (Fig. 10). The same developing of the MR cospectrum was detected compared to the MR cospectrum of $\overline{w'\theta'}$ (Fig. 8). As the moisture flux was directed upwards, a downward flux was observed at a time scale of 10 s and again upwards at 20-40 s. Around a wavelength of 7-8 s a transition from the positive moisture flux into a negative contribution was observed in the wavelets. Within the time series this wavelet gap scale varied and gave evidence for some inhomogeneity of the flux.

6. CONCLUSIONS

Multiresolution decomposition of the heat and moisture flux proofed to be a suitable tool to define a gap time scale between the turbulent and mesoscale flux. Analysing 14 averaged MR cospectra (measured during 5 different flights) resulted in a gap scale range for the heat fluxes between 5 and 30 s ($\approx$ 200-1200 m). The range of gap time scales for the moisture fluxes was slightly smaller, between 6-20 s. This was probably due the the smaller variation of the moisture fluxes between the analysed data records.

The first peak in the MR cospectrum was related to the scale of the main transporting eddies. This time scale of 0.32 s (12-14 m) was the same for almost all the records. No significant differences were found between the cospectra of the heat or the moisture flux. On one day (flight no. 18) larger peak time scales were found (0.64-1.28 s). A strong LLJ was present at this day and caused a shear layer. This shear layer resulted stronger turbulence compared to the other flights and therefore the peak time scales were larger.

For the averaged cospectra no large differences between H and H_{gap} were detected. Larger values of ΔH for the single cospectra were found, but remained mostly within 20% of H. To be sure to expel all of the mesoscale flux contributions, an appropriate time scale should be used for the flux calculations.

The wavelet transformation was a good method for the verification of the MR cospectral time scales. The wavelet covariance gave additional information about the homogeneity of the flux. The wavelengths responsible for the turbulent transport were the same for $\overline{w'\theta'}$ and $\overline{w'm'}$.

ACKNOWLEDGEMENT

We are much obliged to the Alfred Wegener Institute for Polar and Marine Research, Bremerhaven, Germany who funded the Helipod flights. The Helipod flights aboard the research vessel Polarstern were performed by the Helicopter Service Wasserthal, Hamburg, Germany. The data analysis was funded by the German Government (DFG: Polar Stable Boundary Layer, within “Schwerpunktprogramm Antarktis”, grant no. Ba 1988/1-1).

APPENDIX I: Example comparison wavelet and MR cospectra

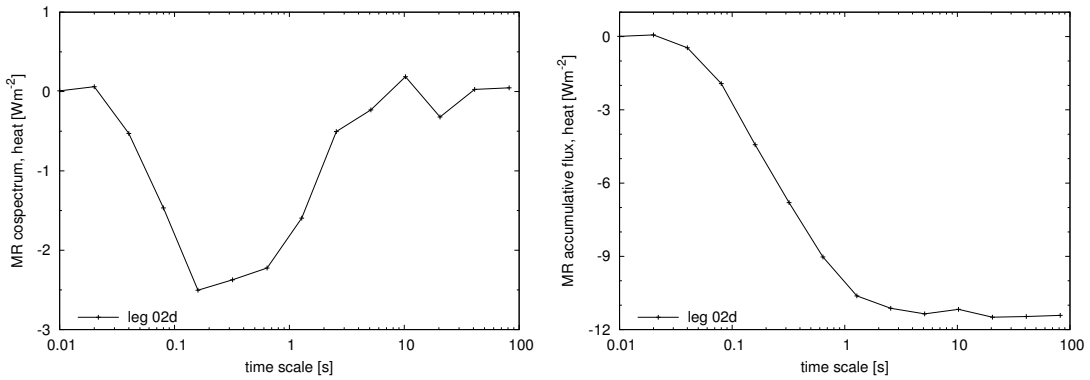

(a) MR cospectrum for the heat flux.

(b) MR accumulative flux for the heat flux.

Fig. 8: MR cospectrum and accumulative flux for a single leg (day 05, leg 02d). The cospectral gap was found around 7 s.

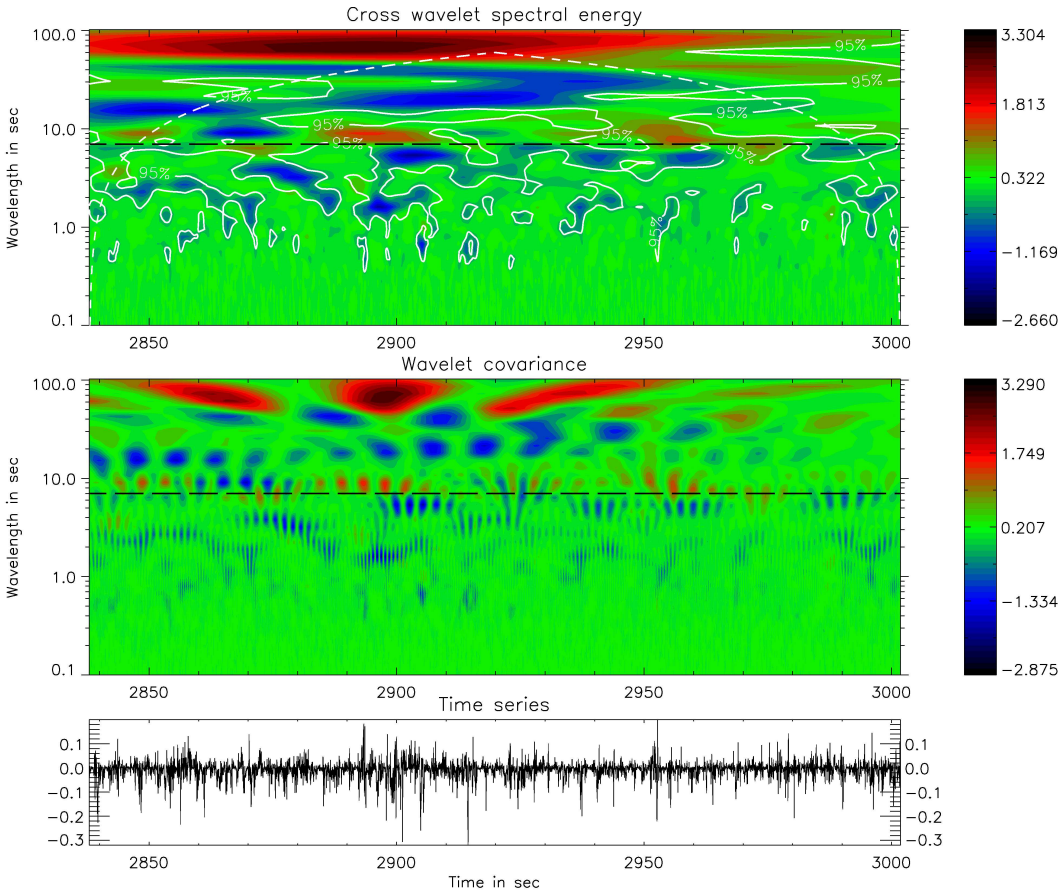

Fig. 9: Wavelet transform (Morlet) of $\overline{w'\theta'}$. Top: Cross wavelet spectrum. The solid white contour line represent the 95% significance level (lag=0.70, red noise). The dashed line represent the cone of influence. Middle: Wavelet covariance. Bottom: The time series of $\overline{w'\theta'}$ [Km s^{-1}]. The black dashed line represents the MR gap scale found by analysing the MR cospectrum, Fig 8. The colorbars indicate the intensity of $\overline{w'\theta'}$.

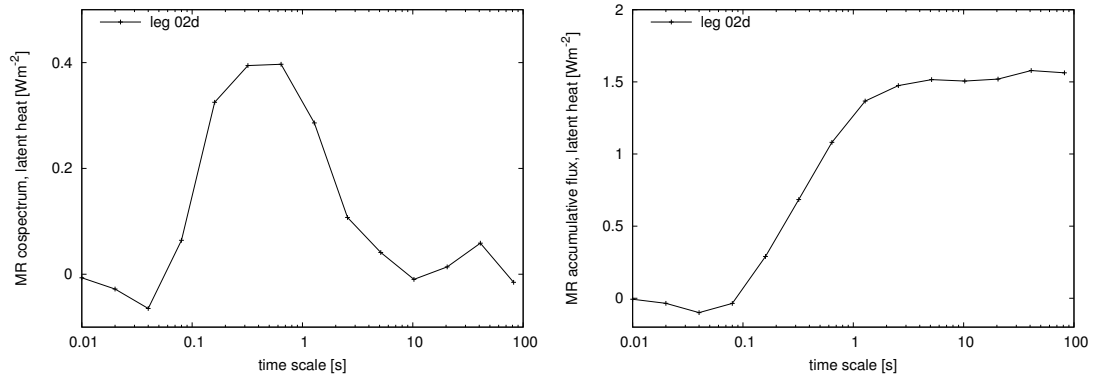

(a) MR cospectrum for the latent heat flux.

(b) MR accumulative flux for the latent heat flux.

Fig. 10: MR cospectrum and accumulative flux for a single leg (day 05, leg 02d). The cospectral gap was found around 8 s.

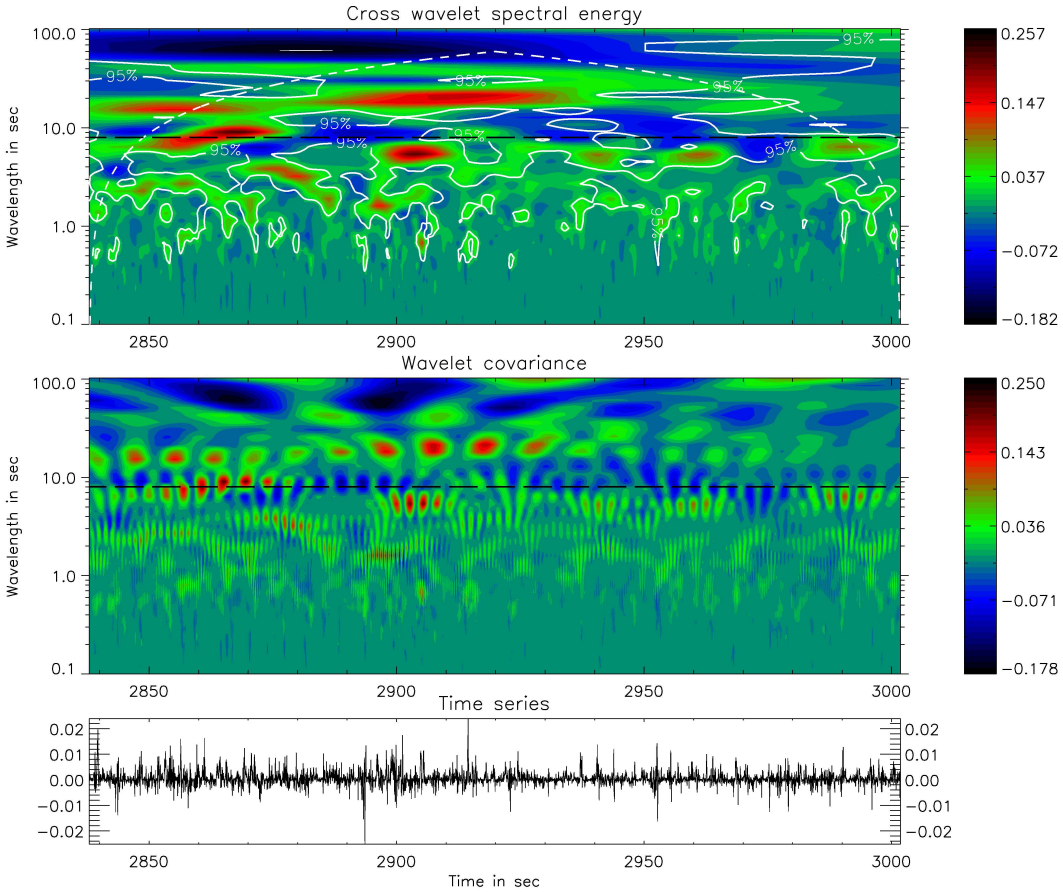

Fig. 11: Wavelet transform (Morlet) of $\overline{w'm'}$. Top: Cross wavelet spectrum. The solid white contour line represent the 95% significance level (lag=0.70, red noise). The dashed line represent the cone of influence. Middle: Wavelet covariance. Bottom: The time series of $\overline{w'm'}$ [Km s^{-1}]. The black dashed line represents the MR gap scale found by analysing the MR cospectrum, Fig 10. The colorbars indicate the intensity of $\overline{w'm'}$.

REFERENCES

Attié, J.-L. and **P. Durand**, **2003**: Conditional wavelet technique applied to aircraft data measured in the thermal internal boundary layer during sea-breeze events. *Boundary-Layer Meteorol.*, **106**, 359–382.

Bange, J., **F. Beyrich**, and **D. A. M. Engelbart**, **2002**: Airborne Measurements of Turbulent Fluxes during LITFASS-98: A Case Study about Method and Significance. *Theor. Appl. Climatol.*, **73**, 35–51.

Bange, J. and **R. Roth**, **1999**: Helicopter-Borne Flux Measurements in the Nocturnal Boundary Layer Over Land - a Case Study. *Boundary-Layer Meteorol.*, **92**, 295–325.

Banta, R., **Y. Pichugina**, and **R. Newsom**, **2003**: Relationship between Low-Level Properties and Turbulence Kinetic Energy in the Nocturnal Stable Boundary Layer. *J. Atmos. Sci., notes and correspondence*, **60**, 2549–2555.

Collineau, S., **Brunet**, and **Y.**, **1993**: Detection of Turbulent Coherent Motions in a Forest Canopy; Part I: Wavelet Analysis. *Boundary-Layer Meteorol.*, **65**, 357–379.

Feigenwinter, D., **1999**: *The Vertical Structure of Turbulence Above an Urban Canopy*. Ph.D. thesis, Universität Basel.

Hagelberg, C. and **N. Gamage**, **1994**: Applications of Structure Preserving Wavelet Decompositions to Intermittent Turbulence: A Case Study. In: *Wavelets in Geophysics*, Academic Press, Inc.

Howell, J. F. and **L. Mahrt**, **1997**: Multiresolution flux decomposition. *Boundary-Layer Meteorol.*, **83**, 117–137.

Katul, G. and **M. Parlange**, **1994**: On the Active Role of Temperature in Surface-Layer Turbulence. *J. Atmos. Sci.*, **15**, 2181–2195.

Kolmogorov, A., **1941**: Local structure of turbulence in an incompressible fluid for very large Reynolds numbers. *Dokl. Akad. Nauk SSSR*, **30**, 299–303.

Mahrt, L., **1999**: Stratified Atmospheric Boundary Layers. *Boundary-Layer Meteorol.*, **90**, 375–396.

Mahrt, L. and **D. Vickers**, **2006**: Extremely weak mixing in stable conditions. *Boundary-Layer Meteorol.*, **in press**, –.

Maraun, D. and **J. Kurths**, **2004**: Cross wavelet analysis: significance testing and pitfalls. *Nonlin. Proc. Geophy.*, **11**, 505–514.

Muschinski, A. and **C. Wode**, **1998**: First In-Situ Evidence for Co-Existing Sub-Meter Temperature and Humidity Sheets in the Lower Free Troposphere. *J. Atmos. Sci.*, **55**, 2893–2906.

Newsom, R. and **R. Banta**, **2003**: Shear-Flow Instability in the Stable Nocturnal Boundary Layer as Observed by Doppler Lidar during CASES-99. *J. Atmos. Sci.*, **60**, 16–33.

Rees, J., **W. Staszewski**, and **J. Winkler**, **2001**: Case study of a wave event in the stable atmospheric boundary layer overlying an Antarctic Ice Shelf using the orthogonal wavelet transform. *Dyn. Atmos. Oceans*, **34**, 245–261.

Salmond, J., **2005**: Wavelet analysis of intermittent turbulence in a very stable nocturnal boundary layer: implications for the vertical mixing of ozone. *Boundary-Layer Meteorol.*, **114**, 463–488.

Sreenivasan, K. and **R. Antonia**, **1997**: The phenomenology of small-scale turbulence. *Annu. Rev. Fluid Mech.*, **29**, 435–472.

Strunin, M. and **T. Hiyama**, **2004**: Applying wavelet transforms to analyse aircraft-measured turbulence and turbulent fluxes in the atmospheric boundary layer over eastern Siberia. *Hydrol. Process.*, **18**, 3081–3098.

Torrence, C. and **G. P. Compo**, **1998**: A Practical Guide to Wavelet Analysis. *Bull. Amer. Meteor. Soc.*, **79**, 61–78.

Vickers, D. and **L. Mahrt**, **2003**: The Cospectral Gap and Turbulent Flux Calculations. *J. Atm. Ocean Tech.*, **20**, 660–627.

Vickers, D. and **L. Mahrt**, **2006**: A solution for flux contamination by mesoscale motion with very weak turbulence. *Boundary-Layer Meteorol.*, **in press**, –.